Key Role of Nitrogen-containing Oxygenated Organic Molecules (OOMs) in SOA Formation Evidenced by OH/NO_3-induced Terpinolene Oxidation

Hongjin Wu[1], Juan Dang[1*], Xiaomeng Zhang[1], Weichen Yang[1], Shuai Tian[2], Shibo Zhang[1*], Qingzhu Zhang[1], Wenxing Wang[1]

1. *Environment Research Institute, Shandong University, Qingdao 266237, China*
2. *Department of Cardiology, The Eighth Affiliated Hospital, Sun Yat-sen University, Shenzhen, Guangdong 518033, China*

Keywords: Oxygenated organic molecules; Terpinolene; SOA formation; Atmospheric oxidation; Atmospheric chemical model

*Corresponding author.
E-mail address: zhangshibo@sdu.edu.cn (Shibo Zhang); dangj@sdu.edu.cn (Juan Dang)

Abstract

Oxygenated organic molecules (OOMs), generated from the oxidation of various biogenic volatile organics with diverse yields, are a great contributor to SOA formation. Terpinolene is an isomeride of limonene, with a high SOA yield. Herein, we investigated the elaborate oxidation mechanism of terpinolene by OH and NO_3, elucidating the new formation mechanism of OOMs and their yield profiles based on the newly-built zero-dimensional chemical model under three typical atmospheric conditions. For terpinolene oxidation by OH, H shift imposes restrictions on continuous autoxidation, instead by the reactions with HO_2/NO/NO_2 resulting in chain termination. For the reaction of terpinolene with NO_3, the transfer of the radical center via bond breaking, triggering a new round of autoxidation, is newly found to be pivotal in the formation of organic nitrate ($RONO_2$) OOMs with high yields. The effective saturation concentration (C^*) of $RONO_2$ OOMs is mostly lower than the OOMs formed by OH oxidation, more easily distributed into the particle phase. The estimated C^* of the generated OOMs is distinctly varied among OOM isomers, which emphasizes the necessity of determining their molecular structures, peculiarly the number of rings. The comparative analysis of OH-initiated (daytime) and NO_3-driven (nocturnal) terpinolene oxidation mechanism, highlighted the formation of $RONO_2$ OOMs, would be conducive to molecular structure identification of OOMs in atmospheric monitoring and atmospheric chemical model refinement.

1 Introduction

In the atmosphere, the multi-generation oxidation reactions of biogenic or anthropogenic volatile organics lead to the formation of oxygenated organic molecules (OOMs) and highly oxygenated organic molecules (HOMs), which are important contributors to secondary organic aerosol (SOA) formation. Given the low volatility, HOMs and OOMs could participate in the nucleation of new particles or condense on the particulate matter to enhance SOA formation. It is well known that SOA has a significant impact on air quality and climate change through scattering and absorbing solar radiation, and serving as cloud condensation nuclei (Shen et al. 2022). Hence, clarifying the formation mechanism of OOMs/HOMs is a vital issue for atmospheric chemistry.

Numerous C10OOMs are generated from monoterpenes ($C_{10}H_{16}$), which are one of the most abundant OOM species in the forests (Bianchi et al. 2017). For instance, the percentage of monoterpene-derived OOMs can be up to 76% in a forested area of southern boreal Finland (Qiao et al. 2023). In urbanized areas of eastern China, the increase in vegetational cover generates a mix of anthropogenic and biological emissions, which contribute to SOA formation (Wang et al. 2020), suggesting that monoterpene OOMs are of concern in urban areas, not only in forested areas (Huang et al. 2016). Concretely, monoterpene OOMs have been detected in recent urban atmospheric observations, approximately 30% of the particulate generation below 10 nm is attributed to monoterpene OOMs in Nanjing (Huang et al. 2016). Measurements in forested areas revealed that monoterpene oxidation products played a dominant role in driving new particle growth (Huang et al. 2016, Mohr et al. 2019), while the atmospheric oxidation mechanisms of monoterpenes, especially the formation of OOMs, have not been fully elucidated.

Previous research mainly focused on the molecular composition (Guo et al. 2022, Liu et al. 2021, Nie et al. 2022), the information on the molecular structure is limited, which hindered a well-grounded understanding of the atmospheric fate of OOMs (Bianchi et al. 2019, Garmash et al. 2020, Kurtén et al. 2017). For instance, when trying to identify the OOMs detected from the field observation, 151 chemical formulas could be categorized as monoterpenes or aromatic hydrocarbons, which would lead to the deviations in OOMs detection and SOA formation

estimation (Qiao et al. 2023). In addition to forming new particles, the relative contribution of OOMs to SOA formation is governed by their net condensation potential, primarily determined by vapor concentrations and volatility (Wang et al. 2022). Generally, the higher the oxygen content of OOMs, the lower their volatility. Given the lack of pure standards, especially for complex multifunctional oxidation products such as OOMs, the measured saturated vapor pressure data are extremely limited. Therefore, the field observations and laboratory studies have employed a two-dimensional volatility basis set (2D-VBS) classification framework to identify the key SOA-contributing components by combining the effective saturation concentration (C^*) and the oxidation state of the oxidation products. In addition, the volatility of the organics with the same molecular formula could vary dramatically due to the structural difference in the functional groups and hydrogen bond (Bianchi et al. 2019, Vasudevan-Geetha et al. 2024). For the estimation of the vapor pressure, Isaacman-VanWertz and Aumont (2021) assumed that the impact of a nitrate group on the vapor pressure is equivalent to a hydroxyl group, which was considered reasonable for the reaction system dominated by R-ONO_2 and peroxynitrates in organic nitrogen gas-phase oxidation products. Besides, according to the chamber experiments and structure-activity relationships, adding -ONO_2 functional groups to C10 and larger molecules could reduce the vapor pressure (Rollins et al. 2013). Currently, the molecular structures of OOMs have not been adequately determined in the field measurements and laboratory investigations, the assessment of their volatility deserves further research.

The atmospheric models typically only consider the representative monoterpene (such as α-pinene), but the SOA yields of different monoterpenes vary widely even with analogous structure (Draper et al. 2015, Friedman and Farmer 2018, Fry et al. 2014, Kurtén et al. 2017, Vasudevan-Geetha et al. 2024). In this work, terpinolene is selected as a model compound due to its high SOA yield. As a kind of cyclic diolefins with an endocyclic and an exocyclic double bond(Griffin et al. 1999), terpinolene has an atmospheric lifetime of 2 hours or less (Corchnoy and Atkinson 1990). The estimated annual emission of terpinolene is roughly 1.3 Tg yr^{-1} (Guenther et al. 2012, Reissell et al. 1999), which is emitted by deciduous tree species such as Sophora japonica and Ginkgo biloba, as well as medicinal plants like Amomum tsaoko seeds (Lindwall et al. 2015). The previous studies have investigated the reaction of terpinolene with O_3 by experimental or theoretical methods (Aschmann et al. 2002, Atkinson et al. 1992,

Atkinson et al. 1990, Herrmann et al. 2010, Kim 2016, Lee et al. 2006, Luo et al. 1996, Orzechowska 2003, Shu and Atkinson 1994, Witter et al. 2002). For the reaction of OH with terpinolene, the rate constant is 2.25×10^{-10} $cm^3molecule^{-1}s^{-1}$ (Corchnoy and Atkinson 1990, Griffin et al. 1999), and the yields of two main products, acetone (32~39%) and 4-methyl-3-cyclohexen-l-one (~26%), have been determined (Hakola et al. 1994, Orlando et al. 2000, Reissell et al. 1999). Notably, the OH-initiated oxidation of terpinolene demonstrates a distinctly higher SOA yield (33% at 5.7 days aging time) compared to α-pinene and limonene (Friedman and Farmer 2018, Surratt et al. 2008). Except for the daytime atmospheric oxidation induced by OH and O_3, NO_3-initiated reactions have been identified as a pivotal nocturnal pathway for terpinolene, with a rate constant of $(6.0\pm3.8)\times10^{-11}$ $cm^3molecule^{-1}s^{-1}$ (Fouqueau et al. 2022). Experimental studies have identified first- and second-generation oxidation products (such as $C_{10}H_{16}O_3$ and $C_8H_{17}N_2O_4$) and proposed that the oxidation mechanism of terpinolene initiated by NO_3 is dominated by NO_3 addition (Fouqueau et al. 2022), with the SOA yield of up to 60% (Corchnoy and Atkinson 1990, Fouqueau et al. 2022, Griffin et al. 1999, Martínez et al. 1999, Stewart et al. 2013). As an important precursor for SOA formation, the OOMs formation mechanisms derived from terpinolene remain unclear, which is critical for deepening the understanding of SOA formation and refining the atmospheric models.

In this study, we combined oxidation mechanism investigation and newly-built kinetic modeling to systematically elaborate OOMs formation from terpinolene oxidation initiated by OH and NO_3 radical, illustrating the yield profiles of OOMs and other products. Additionally, we utilized the functional group contribution method and the molecular formula parameterization method to estimate the saturated vapor pressures of the OOMs to evaluate their contribution to NPF and SOA formation. The comparative investigation of OH-initiated and NO_3-driven oxidation mechanisms of terpinolene, especially for the formation of OOMs, is expected to fill the gap between ambient monitoring of SOA and atmospheric model forecasts.

2 Methods

2.1 Electronic structure and energy calculations

All the quantum chemical calculations were performed utilizing Gaussian 16 software. Conformational optimizations for the reactants, intermediates, transition states, and products

were all carried out at the M06-2X/6-31+G(d, p) computational level. Intrinsic reaction coordinate (IRC) was conducted to ensure that the transition states were related to the matching reactants and products at the same computational level. The single point energies were calculated at M06-2X/6-311++G(3df,3pd) level enhanced the accuracy of energies. The distribution of average local ionization energies (ALIE) was plotted using Multiwfn (Lu and Chen 2012) combined with VMD (Humphrey et al. 1996) for terpinolene to specify its electron-rich sites.

2.2 Kinetics calculations

The rate constants of the reactions are calculated by transition state theory, with the tunneling effect corrected by the Wigner method. The pseudo-first-order rate constants for the bimolecular reactions were derived from the rate constants of RO_2 radicals with HO_2/NO/NO_2 and the concentrations of the reactants under the atmospheric conditions of the urban, suburban, and forested areas. The reaction rate constants were all calculated at 298 K, 1 atm. Using MATLAB, the zero-dimensional chemical models are established based on the oxidation mechanism and kinetics of the alkyl radicals (Ter-R•) produced by the reactions of terpinolene with OH and NO_3 radical.

2.3 Vapor prediction

The functional group contribution method (SIMPOL.1) was used to predict the saturation vapor pressures based on the molecular structure and functional groups of the OOMs (Pankow and Asher 2008). In addition, the molecular formula parameterization method is also employed to calculate the effective saturation concentration(C^*) of the OOMs, which was optimized by Mohr et al. (Mohr et al. 2019) based on the HOMs dataset (Tröstl et al. 2016). The details of these methods are provided in the Supporting Information S1.

3 Results and discussion

For the clarity of the molecular structure and reaction pathways, the carbon atoms of terpinolene were labeled as shown in Fig. S1. Analysis of the ALIE distribution revealed that the two double bonds exhibit the lowest ALIE values, indicating their highest reactivity as the primary reactive sites.

3.1 Initial reactions of Terpinolene with OH/NO_3 radical

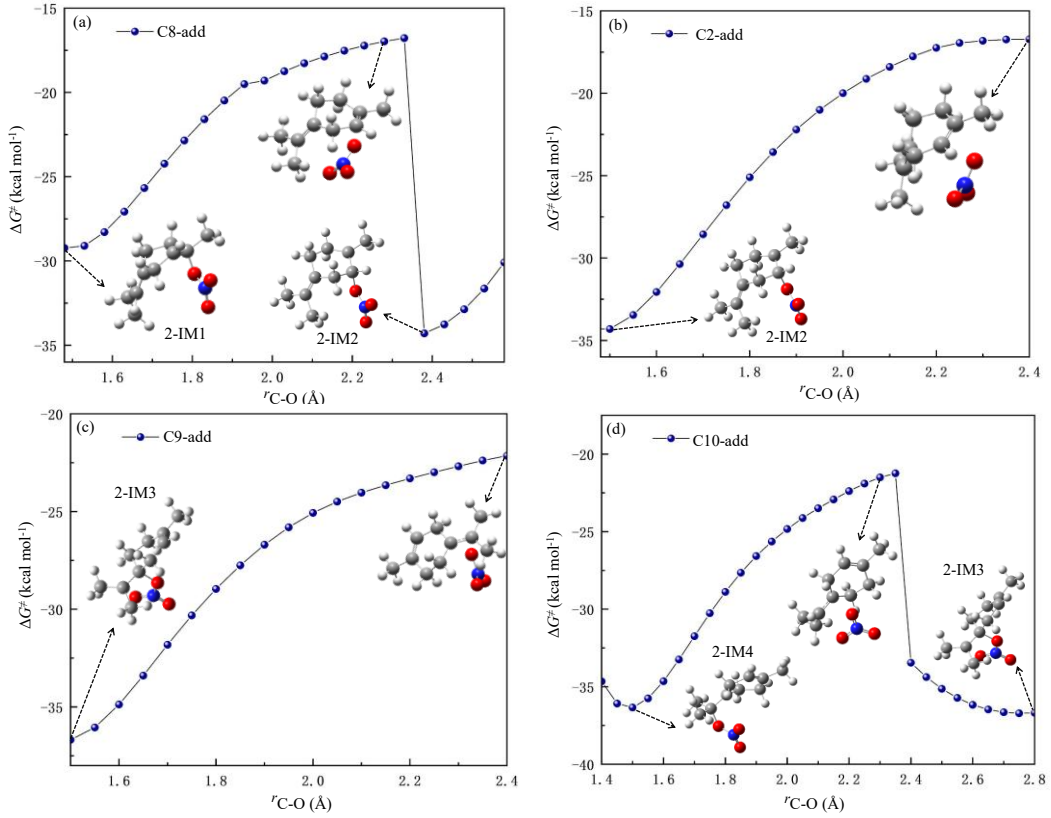

Figure 1. Scanned potential energy surfaces for NO_3 radical addition reactions (unit in kcal mol^{-1})

The initial reactions of terpinolene with OH radical primarily proceed via two mechanisms (Fig. S2), i.e., OH radical addition to two nonconjugated double bonds and H-abstraction by OH radical. All the addition reactions are exergonic and thermodynamically feasible in the atmosphere with the energy barriers of 1.9 ~ 4.7 kcal mol^{-1}, leading to the formation of OH-terpinolene adducts. Analogous to addition reactions, the H-abstraction processes are all exergonic with small free energy barriers (4.9 ~ 9.0 kcal/mol), yielding seven alkyl radicals. The OH addition is dominant over the H-abstraction reaction pathway, which is consistent with the previous laboratory studies (Arey et al. 1990, Orlando et al. 2000, Reissell et al. 1999).

Similar to OH radical, NO_3 radical addition and H-atom abstraction from the carbon chain by NO_3 radical are the initial reaction pathways of terpinolene with NO_3. Notably, NO_3 radical migration is observed in NO_3 addition processes, as shown in the potential energy surface scans at the M06-2X/6-311++G(3df, 3pd) computational level in Fig. 1 (a) and (d), the addition of NO_3 radical to C8 and C10 site produce 2-IM1 and 2-IM4, respectively, which then undergo NO_3 migration to generate 2-IM2 and 2-IM3, overcoming low energy barriers. According to

Fig. 3 (b) and (c), the energy increases with the gradual rising distance of the C-O bond without a saddle point. Therefore, these two addition reactions are considered as barrierless processes. Regarding the H abstraction by NO_3 radical, it can be seen from Fig. S3 that the abstraction reactions are all exothermic (-0.7 ~ -27.8 kcal mol^{-1}), crossing the energy barriers of 1.2 ~ 16.4 kcal mol^{-1} to produce seven different radical intermediates.

3.2 The oxidation of alkyl radicals (Ter-R•) initiated by OH/NO_3 radical

3.2.1 The oxidation of OH-Terpinolene-R• (1-IM4 and 1-IM7)

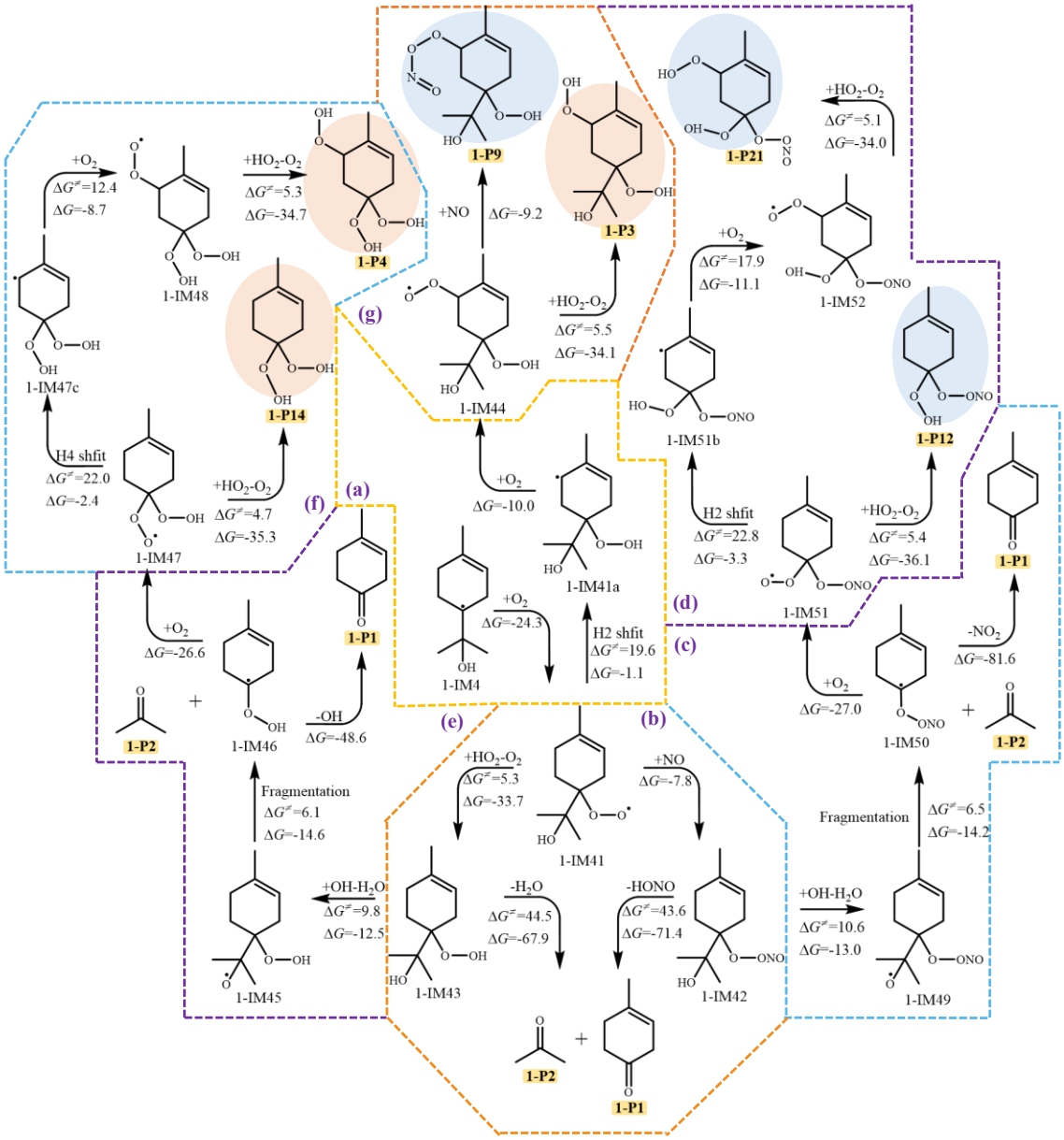

Figure 2. The subsequent reactions of OH-Ter-R• (1-IM4) (unit in kcal mol^{-1}, $RONO_2$ OOMs marked in light blue, nonnitrogenous OOMs marked in lightsalmon)

The alkyl radicals (1-IM4 and 1-IM7) were selected for in-depth study of the atmospheric oxidation mechanism, which are the dominant intermediates formed from OH addition and H-abstraction reactions, respectively. Similar to other C-centered radicals, the reaction with O_2 is the main pathway of 1-IM4 (Peeters et al. 2014). As shown in Fig. 2, 1-IM4 undergoes a rapid barrierless association reaction with O_2, which is exoergic by 24.3 kcal mol^{-1}, leading to the generation of 1-IM41. Three competitive reaction pathways of 1-IM41 are considered: conjugation reaction with NO to generate 1-IM42 under high NO_x conditions, reaction with HO_2 to form the intermediate 1-IM43 under the atmospheric condition of low NOx, and the isomerization reactions, including the cyclization and hydrogen shift. The aforementioned reactions of 1-IM42 and 1-IM43 can both generate 1-P1 and 1-P2, which have been detected in laboratory studies of the reaction of terpinolene with OH radical (Hakola et al. 1994). Unlike the formation mechanism of 1-P2 in the previous experimental research, which proposed that the intermediate generated by the association with NO could directly lead to the formation of 1-P2 and 1-P1 through the removal of NO_2 (Fig. S4) (Orlando et al. 2000, Reissell et al. 1999), we found that HONO is eliminated from 1-IM42 other than NO_2, with a relatively high energy barrier. In addition, 1-IM42 can also undergo H-atom abstraction by OH and the C-C bond cleavage to generate 1-IM50, followed by the elimination of NO_2, yielding 1-P1 and 1-P2. Similarly,1-IM43 can either undergo the removal of H_2O or H-atom abstraction, followed by the fragmentation of the C-C and O-O bond, leading to the formation of the new C7 alkyl radicals (1-IM46), 1-P1 and 1-P2, of which, by comparing the energy barriers, the latter pathway is easier to occur under atmospheric conditions. As depicted in Fig. 2(d),1-IM50 can further react with O_2 to generate the peroxyl radical 1-IM51, which then reacts with HO_2 to generate 1-P12 or triggers a new round of autoxidation, with H2 shift (1,5 H shift) as the rate-determining step, leading to the formation of 1-P21. Analogously, 1-IM46 can undergo O_2 addition to generate a peroxyl radical 1-IM47, ultimately resulting in the generation of 1-P4 and 1-P14. According to the traditional autoxidation mechanism (Fig. 2(a)), 1-IM41 undergoes H2 shift (1,5 H shift) to form 1-IM41a with an energy barrier of 19.6 kcal mol^{-1}, which further reacts with O_2 to produce a new peroxyl radical 1-IM44. Whereas, the subsequent oxidation of 1-IM44 is restricted due to the high energy barriers of the H shift and cyclization reactions (Fig. S6), which cannot occur spontaneously under atmospheric conditions. Therefore, 1-IM44 can

only react with HO_2 to form 1-P3 or react with NO to produce a nitrogenous OOM 1-P9, which have been identified as the major monoterpene-derived C10OOMs in the field observations (Guo et al. 2022, Luo et al. 2023, Zheng et al. 2023). The presence of the endocyclic double bond enables 1-IM41 to undergo cyclization to generate 1-IM41f and 1-IM41g, which are thermodynamically unfavorable under atmospheric conditions (Fig. S5).

The subsequent reaction pathway of 1-IM7 is initiated with O_2 addition to form the peroxyl radical 1-IM71, which further reacts with HO_2 to generate 1-IM74, followed by the hydrogen abstraction by OH radical and OH elimination to yield 1-P7 (Fig. 3(b)). 1-IM71 can also react with NO, consecutively proceeding with NO_2 elimination and the binding with O_2 to produce the peroxyl radical 1-IM78. As shown in Fig. 3(c), 1-IM78 can sequentially react with HO_2/NO to generate 1-P8 and 1-P11, respectively. In addition, 1-IM78 can also undergo H4 shift (1,6 H shift) to form 1-IM78d, which subsequently reacts with O_2 to generate a new peroxyl radical 1-IM79, eventually leading to the production of 1-P13, which has been detected in the field observation and the laboratory studies of limonene oxidation by OH (Luo et al. 2023, Zheng et al. 2023). Furthermore, the peroxyl radical 1-IM79 can react with NO/NO_2 to produce organic nitrate ($RONO_2$) OOMs 1-P15 and 1-P16. Additionally, the peroxyl radical 1-IM71 undergoes the H4 shift (1,5 H shift) and the association with O_2 to produce a new peroxyl radical 1-IM72, which can further react with HO_2 to generate the OOM 1-P5, or react with NO/NO_2 to form 1-P17 and 1-P18, respectively (Fig. 3(e)). Analogously, Fig. 3(f) indicates that the peroxyl radical 1-IM72 can undergo a subsequent H4 shift (1,5 H shift) reaction, initiating an additional autoxidation cycle to generate more OOMs. The isomerization reactions involved in the reaction pathways are displayed in Section. S3 of Supporting Information, and the major products from the reactions of terpinolene with OH/NO_3 are summarized in Sect. S6.

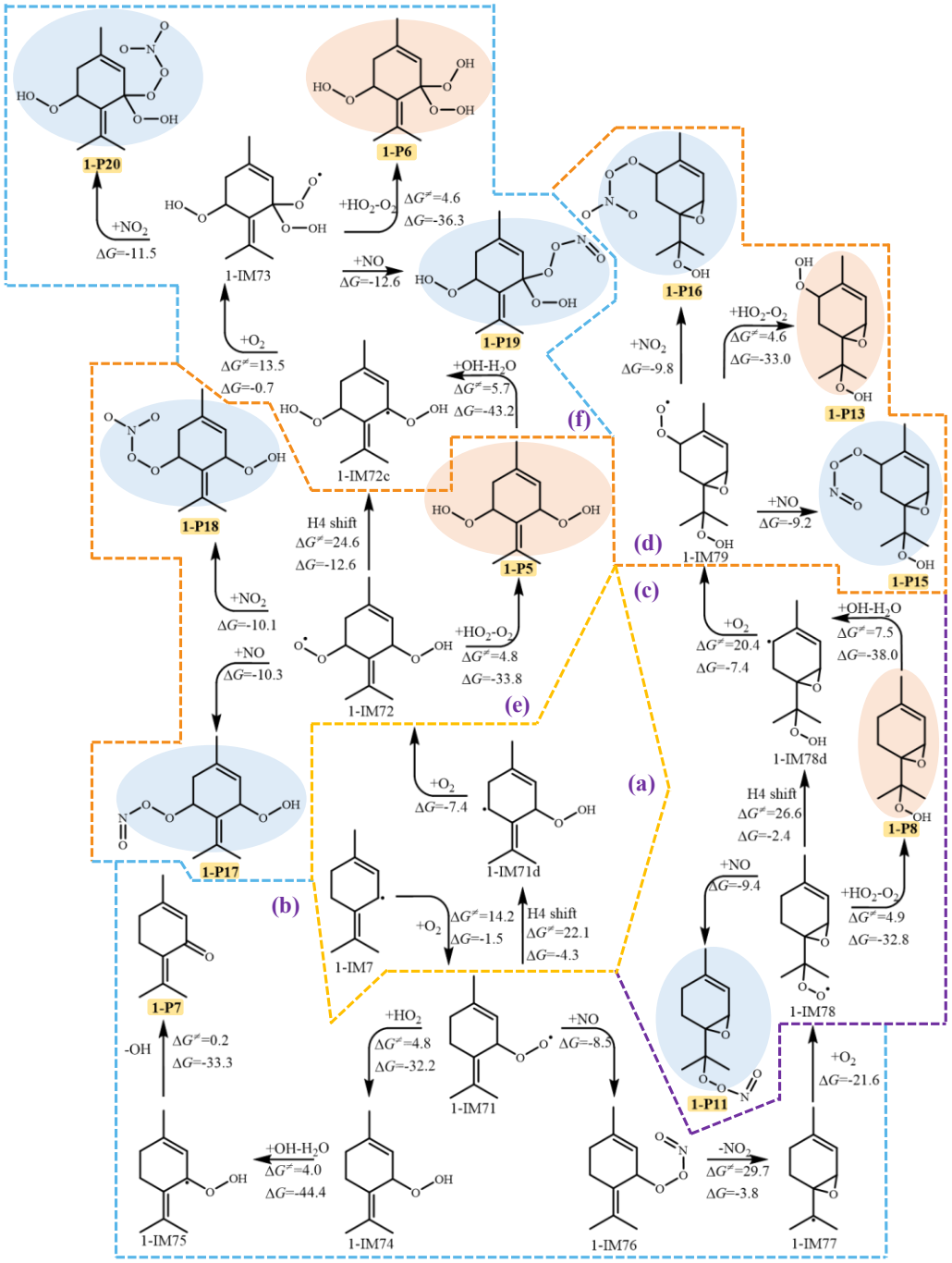

Figure 3. The subsequent reactions of OH-Ter-R• (1-IM7) (unit in kcal mol^{-1}, $RONO_2$ OOMs marked in light blue, nonnitrogenous OOMs marked in lightsalmon)

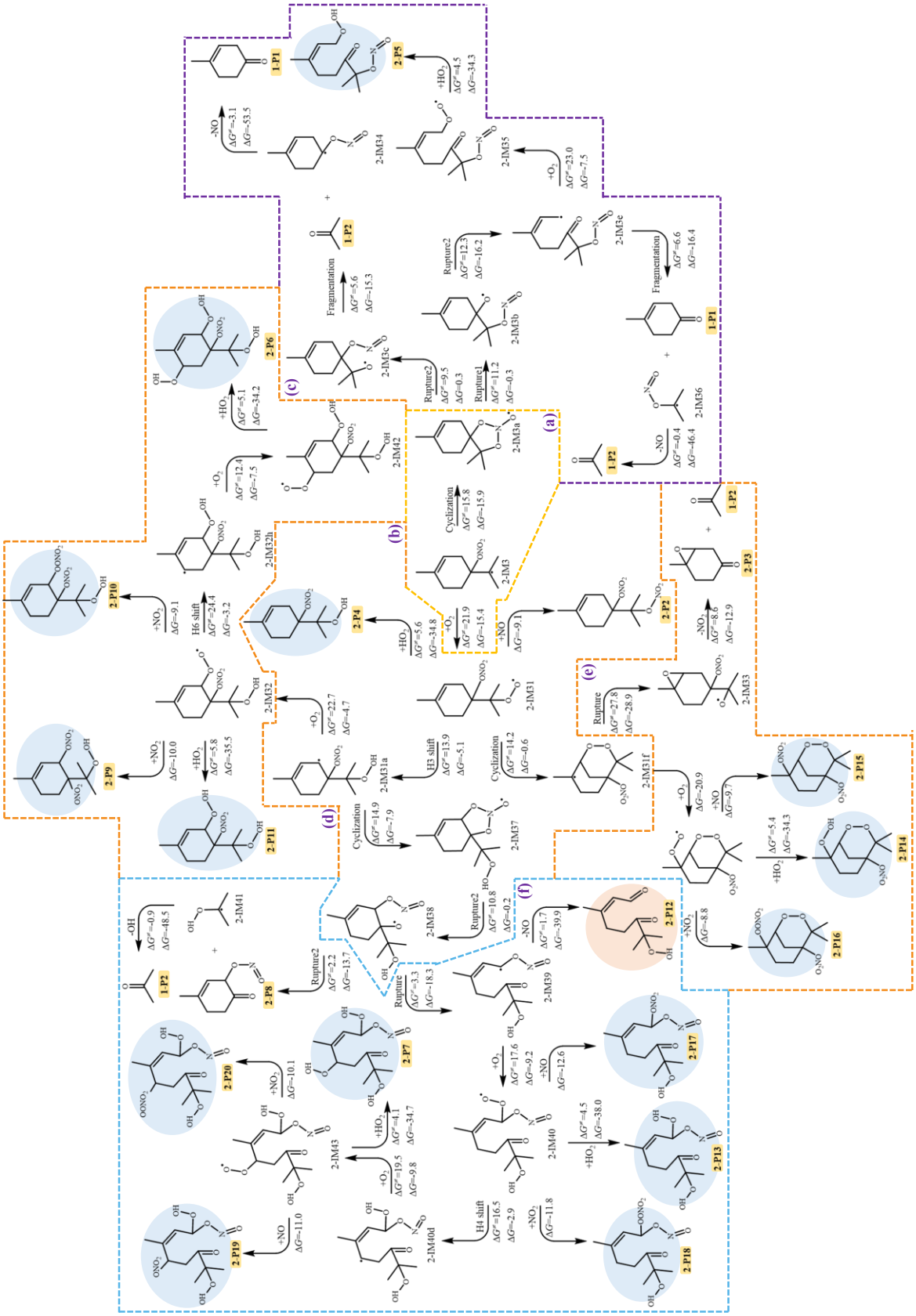

Figure 4. The subsequent reactions of NO_3-Ter-R• (2-IM3) (unit in kcal mol^{-1}, $RONO_2$ OOMs marked in light blue, nonnitrogenous OOMs marked in light salmon)

3.2.2 The atmospheric oxidation of the NO_3-Terpinolene-R• (2-IM3)

The dominant intermediate NO_3-Ter-R• (2-IM3) is prone to cyclization to form a bicyclic alkoxyl radical (2-IM3a), as shown in Fig. 4. Due to the instability of the N-O bond, 2-IM3a undergoes the rupture of the O-N bond to produce 2-IM3b or 2-IM3c, which both subsequently proceed with the fragmentation and NO elimination to generate 1-P1 and 1-P2. Besides, Fig. 4(c) indicates that the radical center of 2-IM3b migrates from the oxygen atom to the carbon atom via C-C bond breaking, and consecutively reacts with O_2 and HO_2 to generate 2-P5. Similar to the intermediate OH-Ter-R• (1-IM4), 2-IM3 also reacts with O_2 to generate the first-generation peroxyl radical (2-IM31), which further reacts with HO_2 to generate 2-P4 (Fig. 4(b)). As the presence of an endocyclic double bond, 2-IM31 proceeds with the cyclization to produce 2-IM31f with a barrier of 14.2 kcal mol^{-1}, followed by O-O bond rupture and NO_2 removal to form 2-P3 and 1-P2, which have been detected in the laboratory studies for the oxidation of terpinolene by NO_3 radical (Fouqueau et al. 2022). Moreover, as shown in Fig. 4(e), the bicyclic alkyl radical 2-IM31f ulteriorly reacts with O_2 to form a new peroxyl radical, resulting in the formation of multiple OOMs.

Among all the H shift reaction pathways (Fig. S11), H3 shift (1,5 H shift) is the dominant reaction pathway to form 2-IM31a, which continues to react with O_2 to produce 2-IM32 or proceeds with a cyclization reaction to generate an alkoxy radical 2-IM37. The peroxyl radical 2-IM32 can further undergo the bimolecular reactions with HO_2/NO/NO_2, or continue the autoxidation to produce 2-P6, as shown in Fig. 4(d). For the subsequent reactions of the alkoxy radical 2-IM37, the cleavage of the O-N and C-C bond occurs, followed by OH removal, leading to the formation of 2-P8 and 1-P2. In addition, 2-IM37 can also undergo the rupture of the O-N and C-C bonds to produce the intermediate 2-IM39, which can react with O_2 or eliminate NO to generate a new peroxyl radical 2-IM40 or 2-P12. Subsequently, 2-IM40 proceeds with the autoxidation mechanism driven by H4 shift (1,6-H shift) and then the reaction with HO_2 to generate 2-P7 and 2-P13. The peroxyl radicals (2-IM40 and 2-IM43) can also react with NO/NO_2 to produce $RONO_2$ OOMs, including 2-P17, 2-P18, 2-P19, and 2-P20. According to the field observation of OOMs at a coastal background site in Hong Kong, 2-P6 and 2-P9~2-P20 have been detected (Zheng et al. 2023). Moreover, the MT-mixed-OOMs identified in the

atmospheric monitoring over eastern China's megacities, such as 2-P9, 2-P10, 2-P15 ~ 2-P18, are considered to be generated by the reactions of the peroxyl radicals with NO/NO_2, which is in accordance with the reaction pathways we discussed above (Liu et al. 2023). For clarity, the above-mentioned products that could have been detected in field observations are all summarized in the Supplementary Section. S6.

3.3 Modeling of the yield profiles of OOMs and other main products

Based on the aforementioned oxidation mechanism of terpinolene by OH and NO_3 radical, the thermodynamically feasible reaction pathways were determined, and a zero-dimensional chemical model was further established to calculate the time-dependent fractional yields of the intermediates and major products including OOMs under three atmospheric conditions: (a) in a urban area (50 ppb NO, 39 ppb NO_2, 1 ppt HO_2), (b) in a suburban area (3 ppb NO, 9 ppb NO_2, 3 ppt HO_2), and (c) in a forested area (0.5 ppb NO, 4 ppb NO_2, 40 ppt HO_2) (Guo et al. 2024, Kieloaho et al. 2013, Klemm et al. 2006, Lew et al. 2020, Ma et al. 2019, Mao et al. 2010, Mavroidis and Ilia 2012, Mazzeo et al. 2005, Zhang et al. 2022). Based on the bimolecular reaction rate constants of the RO_2 with NO (9.0×10^{-12} cm^3 $molecule^{-1}$ s^{-1}), NO_2 (1.10×10^{-11} cm^3 $molecule^{-1}s^{-1}$) and HO_2 (1.7×10^{-11} cm^3 $molecule^{-1}$ s^{-1}) and the C-centered radicals with O_2 (6.0×10^{-12} cm^3 $molecule^{-1}s^{-1}$) (Atkinson and Arey 2003, Boyd et al. 2003, Saunders et al. 2003, Wang and Wang 2016, Wu et al. 2015), the pseudo-first-order rate constants were determined and inputted into the model, as summarized in Supplementary Sect. S4. In the urban area, the calculated pseudo-first-order rate constant k'_{RO2+NO} (1.11×10^{1} s^{-1}) is significantly larger than $k'_{RO2+HO2}$ (4.18×10^{4} s^{-1}). Whereas, under the atmospheric condition of the forested area, where NO concentration is 0.5ppb, $k'_{RO2+HO2}$ (1.67×10^{-2} s^{-1}) becomes comparable with k'_{RO2+NO} (1.11×10^{-1} s^{-1}).

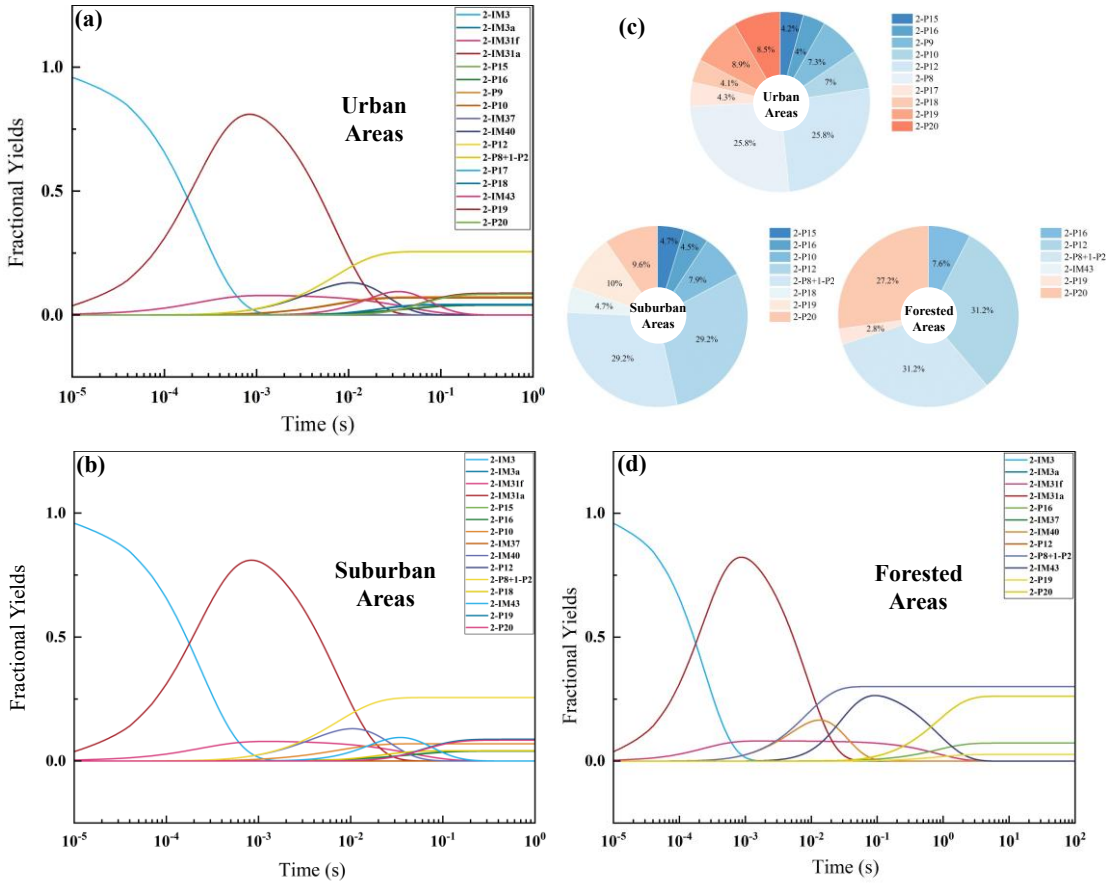

Figure 5. The modeled time-dependent fractional yields of important species generated from the subsequent reactions of NO_3-Ter-R•(2-IM3) under the atmospheric conditions of urban areas (a), suburban areas (b), forested areas (d) (Species with yields 1% excluded).

The time-dependent fractional yield of the major products from the oxidation of NO_3-Ter-R• (2-IM3) is shown in Fig. 5. The rate constants of the rate-determining steps for the generation of 2-IM3a, 2-IM31a, and 2-IM31f from 2-IM3 were calculated to be 27.1 s^{-1}, 3.83 × 10^3 s^{-1}, and 3.42 × 10^2 s^{-1}, respectively. Compared to the bimolecular reaction pathways for the production of 2-P4 and 2-P2, unimolecular reactions are more dominant, among which, 2-IM31a generated by the hydrogen shift reaction is the predominant intermediate. As shown in Fig. 5(a), the fractional yield of 2-IM31a is sharply increased to 80% at ~ 10^{-3} s in the urban area, accompanied by a rise in the yield of 2-IM31f to ~ 8.0%. Subsequently, the yield of 2-IM31a declines rapidly to ~ 0%, along with the rising yield of 2-P8, 2-P12, and 1-P2 to level off at ~26% at 10^{-1}s. Sequentially, 2-IM31a undergoes the cyclization and O_2 addition to produce 2-IM40, which is stabilized at ~ 13% at around 10^{-2} s. The continuous oxidation of 2-IM40 leads to the increasing yield of 2-IM43 via the autoxidation driven by the H4 shift reaction (4.43 ×

10 s^{-1}). Ultimately, the OOMs 2-P19 and 2-P20 are formed from the reactions of 2-IM43 with NO and NO_2, with their yields leveling off at 1 s. As indicated in Fig. 5 (b) and (d), the intermediates generated by the unimolecular reactions (such as 2-IM31a, 2-IM43, etc.) are also dominant. In urban and suburban areas, the yields of 2-P19 and 2-P20 are comparable; however, in the forest area, 2-P20 generated by the peroxyl radical and NO_2 are the main $RONO_2$ OOMs, with the yield of 27.2%. Additionally, in the urban area, the yields of 2-P9 and 2-P17 produced by the peroxyl radicals and NO are 7.3% and 4.3%, respectively, while those are all below 1% in suburban and forest areas. The reactions of peroxyl radicals with HO_2 increase the yield of 2-P7(< 1%) in the forest and suburban area, but can't compete with those of peroxyl radicals with NO/NO_2, which leads to the production of 2-P19 and 2-P20. As summarized in Fig. 5 (c), under these three atmospheric conditions, 2-P8, 2-P12, 2-P19, and 2-P20 are the main OOMs with relatively high yields, while 2-P10 is the major OOM in the urban and suburban areas (7% and 7.9%, respectively). The total yield of the OOMs (2-P15 and 2-P16) generated by the subsequent oxidation of 2-IM31f produced by the cyclization reaction is approximately 8~10% in the urban and suburban area, while the OOM in the forested area (2-P16) has a yield of 7.6%.

As shown in Fig. S16, as the main oxidation product, the yields of 1-IM42 are 96.8% and 64.1% in the urban and suburban areas, respectively, followed by 1-P9. In the forested area, the main oxidation intermediate of 1-IM4 is 1-IM41a, generated by the first hydrogen shift reaction, which undergoes bimolecular reactions with HO_2/NO to produce 1-P3 (9.7%), 1-P9 (64.7%), 1-IM42 (22.2%), and 1-IM43 (3.3%). In Fig. S17, under three atmospheric conditions, the yield of 1-IM76 is over 80%, synchronously, being one of the main oxidation products. The fractional yield of 1-P7 and 1-P18 is enhanced to 12% and 2%, respectively, in forested areas. By contrast, there is a significant difference in the yields of OOMs produced from the oxidation of terpinolene by OH and NO_3 radical, mainly due to the different oxidation pathways.

3.4 Volatility distribution of OOMs

The saturation vapor pressures of OOMs can affect their condensation process, which is closely related to SOA formation. Low volatility organic compounds (LVOC) and extremely low volatility organic compounds (ELVOC) have been demonstrated to be a significant contributor to the growth of a large proportion of the new particles, with a minor contribution

from semi-volatile organic compounds (SVOC) (Mohr et al. 2017). Herein, based on the chemical formula and functional groups of the OOMs generated from the oxidation of terpinolene by OH and NO_3, the saturation vapor pressures of the OOMs were firstly predicted using SIMPOL.1 functional group contribution method (Pankow and Asher 2008, Valorso et al. 2011). It was then converted to the effective saturation concentration (C^*) for further comparison with the estimation by the optimized molecular formula parameterization method (Mohr et al. 2019).

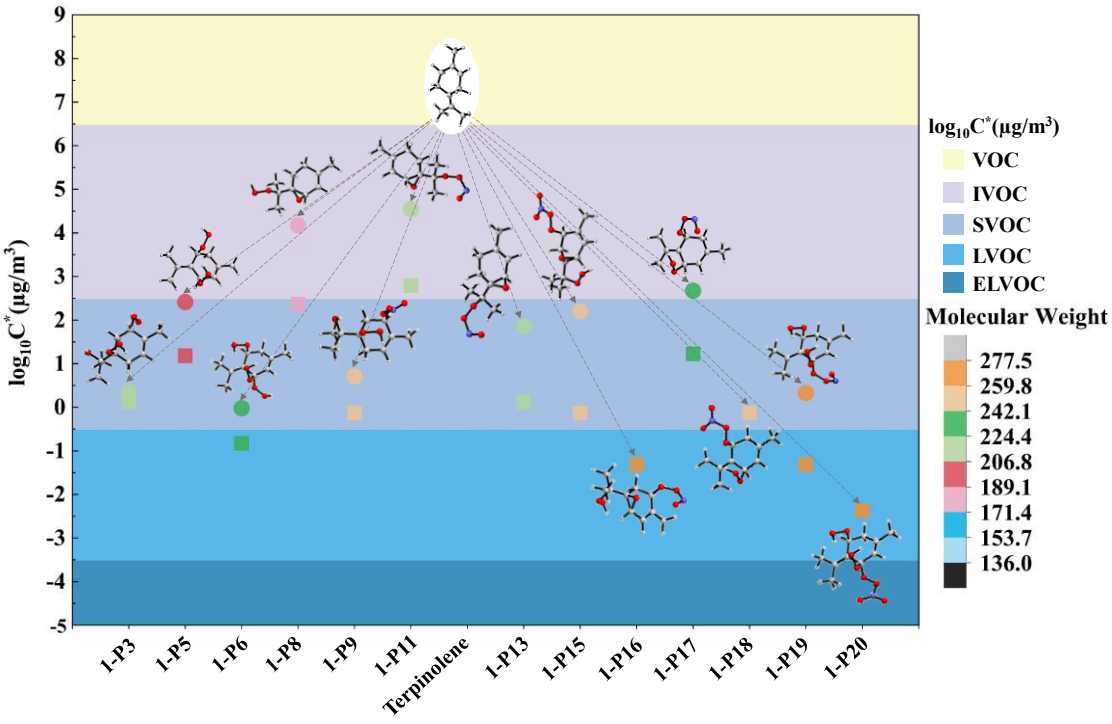

Figure 6. The molecular weight ranges and volatility classifications of C10-OOMs generated from OH-Ter-R•(1-IM4 and 1-IM7) oxidation. (Volatility prediction methods: (○) the functional group contribution method (SIMPOL.1), (□) the molecular formula parameterization method)

As shown in Fig. 6, the OOMs generated from the oxidation of terpinolene with OH are mainly IVOC, SVOC, and LVOC. Noteworthily, the results obtained from both methods indicate that most of the OOMs belong to SVOC and LVOC, among which, 1-P6, 1-P16, 1-P19, and 1-P20 are categorized as LVOC by the molecular formula parameterization method, while 1-P6 and 1-P19 are identified as SVOC, according to the functional group contribution method. From the analysis of the atmospheric oxidation mechanism of terpinolene by OH, it can be found that these four OOMs are generated by the subsequent oxidation of the intermediate 1-IM7 produced by the H-atom abstraction reaction, and the $RONO_2$ OOMs (1-

P16, 1-P19, and 1-P20) are produced by the reactions of peroxyl radicals with NO/NO_2. 1-P16 is generated by the reaction of NO_2 with a new peroxyl radical formed by the autoxidation of the peroxyl radical containing a C-O-C ring, which is derived from the reaction of IM7 with NO/O_2. In the previous analysis, we also emphasized the importance of this pathway for the generation of OOMs, due to the existence of $C=C(CH_3)_2$ double bond in the terpinolene molecule, unlike the molecular structures of the products generated from NO_2 elimination in previous studies, a C-O-C ring is formed, leading to the generation of a new alkyl radical, which is conducive to the generation of OOMs.

As revealed in Fig. 7, most of the OOMs generated from the oxidation of terpinolene by NO_3 are nitrogenous OOMs, except for 2-P12. The results obtained from the functional group contribution method indicate that the majority of the nitrogenous OOMs are within the range of SVOC, with only 2-P6, 2-P7, and 2-P19 assigned to LVOC. According to the molecular formula parameterization method, most of the $RONO_2$ OOMs belong to LVOC, except for 2-P19 and 2-P20 sorted as ELVOC. Concretely, 2-P6 is the oxidative product of the adduct 2-IM3 via twice H shifts (1,5- and 1,6-H shift). For the formation of 2-P7, 2-P19, and 2-P20, the alkoxyl radical 2-IM37 undergoes the cleavages of the O-N and C-C bond and the further reaction with O_2 to produce a new peroxyalkyl radical, ultimately producing 2-P7, 2-P19, and 2-P20 through 1,6-H shift, the reaction with NO and NO_2, respectively. Overall, compared to the generated OOMs induced by OH, the effective saturation concentration (C^*) of OOMs derived from the oxidation by NO_3 is generally lower, being more easily distributed into the particle phase. It should be noted that there existed a significant difference in the volatile classification of 2-P14 and 2-P15 containing bicyclic structure utilizing these two methods, even crossing the SVOC range.

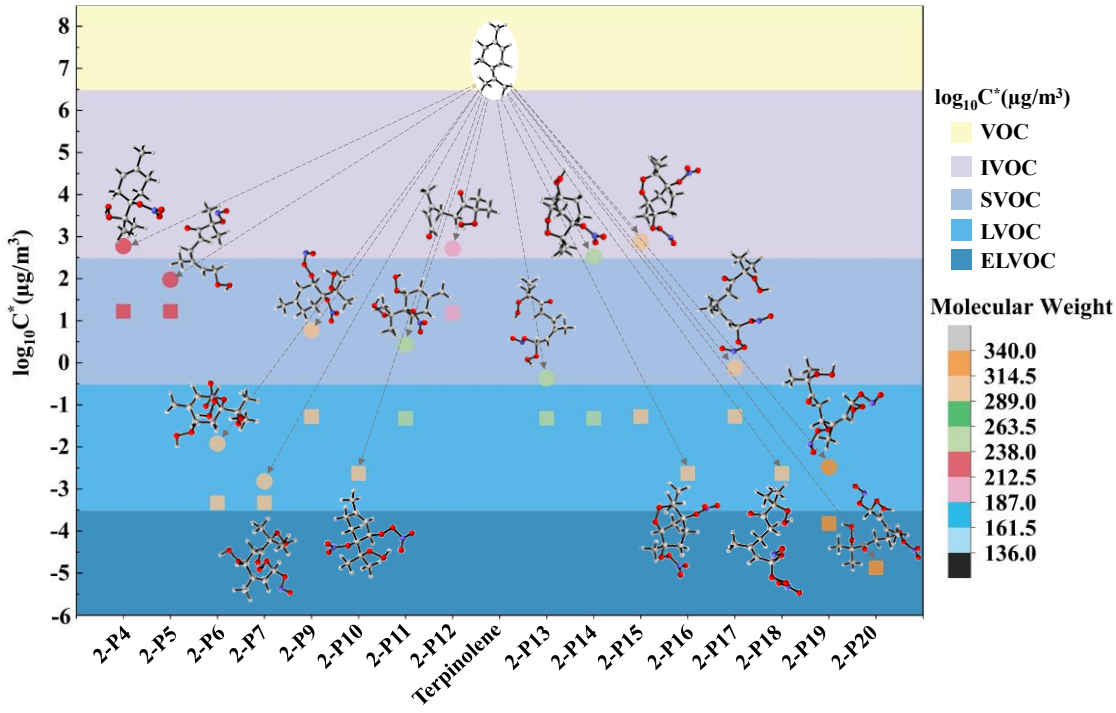

397

398 **Figure 7.** The molecular weight ranges and volatility classifications of C10-OOMs generated
399 from NO_3-Ter-R• (2-IM3) oxidation. (Volatility prediction methods:(○) the functional group
400 contribution method(SIMPOL.1), (□) the molecular formula parameterization method)

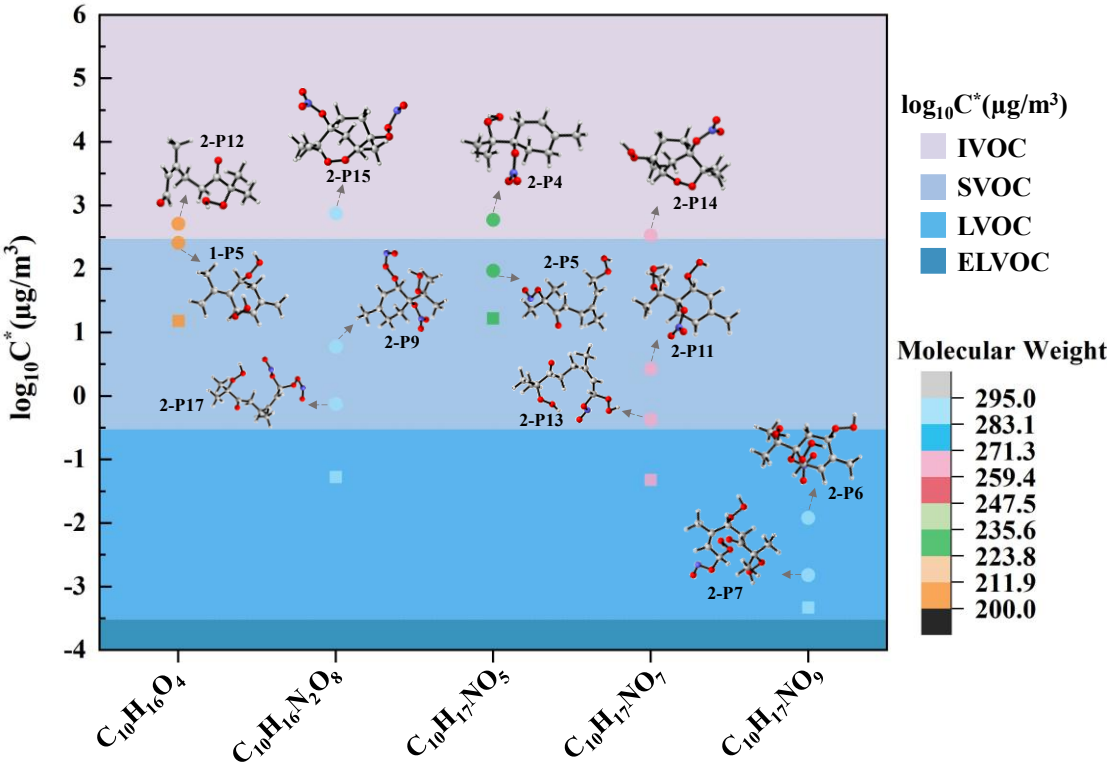

401

402 **Figure 8.** The molecular weight ranges and volatility classifications of C10-OOMs isomers.
403 (Volatility prediction methods: (○) the functional group contribution method(SIMPOL.1), (□)
404 the molecular formula parameterization method)

Based on the molecular structures of each OOMs obtained from quantum chemical calculation, five groups of isomers were emphatically discussed, as shown in Fig. 8, the C^* values of OOMs estimated by the molecular formula parameterization method are generally smaller compared to the results obtained from the functional group contribution method, possibly leading to a distinct underestimation of the saturated vapor pressure, which could affect the accurate assessment of the gas-particle partitioning of OOMs. By contrast, the difference in the effective saturation concentrations of the nitrogen-free OOMs (2-P12 and 1-P5) is small, while those for the other four groups of $RONO_2$ OOMs isomers exhibit evident differences. Moreover, for the nitrogen-free OOMs (2-P12 and 1-P5), the saturated vapor pressure of 1-P5 with a cyclic structure was relatively lower. For the $RONO_2$ OOMs (the other four groups), the effective saturation concentrations of the isomers in each group follow the rule, i.e., the bicyclic structure > the monocyclic structure > the acyclic structure, which implies that the ring-opening reaction could have an important influence on the generation of the low-volatile products. According to the previous findings of the vital role of isoprene nitrates in new particle formation in the upper troposphere over Amazon, the $RONO_2$ OOMs could contribute significantly to SOA formation (Curtius et al. 2024).

4 Conclusion and atmospheric implications

In this work, the atmospheric oxidation mechanism of terpinolene by OH and NO_3 was comprehensively investigated, expounding the formation pathways of OOMs and their molecular structures, indirectly corroborated by the available field observations and laboratory studies. Based on the reaction mechanism, the zero-dimensional chemical model was established to clarify the yield profiles of the main products including OOMs under three typical atmospheric conditions. In addition, the saturation vapor pressures of OOMs were estimated by the SIMPOL.1 method and the molecular formula parameterization method to evaluate their contributions to SOA formation.

We found that the first-generation peroxyl radical (1-IM71), resulting from the H-atom abstraction reaction pathway of terpinolene by OH, plays a pivotal role in the formation of C10OOMs. 1-IM71 can undergo twice H shift or the reaction with NO to form a cyclic peroxy radical (1-IM79), ultimately leading to the production of low volatile OOMs (such as 1-P19, 1-

P20, and 1-P16). Among the products, the yields of 1-IM76 account for the large proportions under three atmospheric conditions. Whereas, the first-generation peroxyl radical formed by the OH addition reaction of terpinolene can only proceed with one H shift continued with bond breaking, resulting in the formation of C7OOMs. According to the yield profiles, 1-P9 are the main oxidation products with yields of more than 30% in suburban and forested areas.

For the oxidation of terpinolene by NO_3, the first-generation peroxyl radical derived from NO_3 addition can also undergo H shift, followed by the cyclization, the rupture of O-N bond and C-C bond, thereby the radical center is migrated, triggering a new round of autoxidation driven by the hydrogen shift reaction to produce $RONO_2$ OOMs, with the total yields of 2-P18, 2-P19 and 2-P20 over 20%. Analogously, the adduct generated by NO_3 addition to terpinolene can also produce C10OOMs (2-P5) via cyclization and the cleavage of O-N and C-C bonds. Therefore, the reaction pathway of achieving the transfer of the radical center via bond breaking is a newly identified but important mechanism for the formation of OOMs except for H shift, which could be applicable to the oxidation of other terpenoids.

The generated OOMs by atmospheric oxidation of terpinolene are mainly IVOC, SVOC, LVOC, and some ELVOC, and there is a distinct difference in the effective saturation concentration of the OOM isomers. Compared with the OOMs (mostly I/SVOC) generated from the oxidation of terpinolene by OH radical, the formed $RONO_2$ OOMs (mainly S/LVOC) via the reaction of terpinolene with NO_3 have lower volatility with more potential to contribute to SOA formation. It could be indirectly proved by the measurements in urban atmospheres, the concentrations of organic nitrate ($RONO_2$) OOMs dominated the total OOMs during four seasons (Yuan et al. 2024), highlighting its significance in atmospheric chemistry.

Given the multitude of OOMs formed in the atmosphere, their molecular structures (existing numerous isomers) and formation pathways remain unclear. The findings of this work would be conducive to illuminating the formation mechanism of OOMs by terpene oxidation in the atmosphere and the measurements in the laboratory and field sites. However, it should be noted that the yields of OOMs calculated by the zero-dimensional chemical model could have some uncertainties, derived from the uneven distribution of pollutants, the neglect of advection, diffusion, and meteorological factors, incomplete chemical mechanisms, the errors of initial conditions, time step size, and numerical integration, etc. Therefore, well-integrated

models are needed to clarify the coupling of OOMs formation with multiple factors, achieving more accurate predictions.

Code/Data availability

The data and code for quantum chemical calculations and zero-dimensional chemical models used in this study are available upon request.

Supporting Information Available

Detailed information on Fig. S1-S15 and Table S1-S4 is all provided in the supporting information.

Author contributions

JD and HW conceived and designed the study and wrote the original draft. HW performed the data analysis and created the figures; XZ, WY, ST, and SZ collected the dataset. ST and JD developed the model. SZ, QZ, and WW reviewed and edited the manuscript. All authors participated in the discussion and review of the manuscript.

Competing interests

The contact author has declared that none of the authors has any competing interests.

Acknowledgments

This work was supported by the National Natural Science Foundation of China (No. 22006095, 52106169, 22236004), the China Postdoctoral Science Foundation (No. 2021M690097), and the Future Plan for Young Scholars of Shandong University.

Reference

Arey, J., Atkinson, R. and Aschmann, S.M. (1990) Product Study of the Gas-Phase Reactions of Monoterpenes With the OH Radical in the Presence of NOx. Journal of Geophysical Research-Atmospheres 95(D11), 18539-18546.

Aschmann, S.M., Arey, J. and Atkinson, R. (2002) OH radical formation from the gas-phase reactions of O3 with a series of terpenes. Atmospheric Environment 36(27), 4347-4355.

Atkinson, R. and Arey, J. (2003) Atmospheric Degradation of Volatile Organic Compounds. Chemical Reviews 103(12), 4605-4638.

Atkinson, R., Aschmann, S.M., Arey, J. and Shorees, B. (1992) Formation of OH Radicals in the Gas Phase Reactions of O3 With a Series of Terpenes. Journal of Geophysical Research-Atmospheres 97(D5),

6065-6073.
Atkinson, R., Hasegawa, D. and Aschmann, S.M. (1990) Rate Constants for the Gas-Phase Reactions of O3 with a Series of Monoterpenes and Related Compounds at 296±2 K. International Journal of Chemical Kinetics 22(8), 871-887.
Bianchi, F., Garmash, O., He, X.C., Yan, C., Iyer, S., Rosendahl, I., Xu, Z.N., Rissanen, M.P., Riva, M., Taipale, R., Sarnela, N., Petäjä, T., Worsnop, D.R., Kulmala, M., Ehn, M. and Junninen, H. (2017) The role of highly oxygenated molecules (HOMs) in determining the composition of ambient ions in the boreal forest. ATMOSPHERIC CHEMISTRY AND PHYSICS 17(22), 13819-13831.
Bianchi, F., Kurtén, T., Riva, M., Mohr, C., Rissanen, M.P., Roldin, P., Berndt, T., Crounse, J.D., Wennberg, P.O., Mentel, T.F., Wildt, J., Junninen, H., Jokinen, T., Kulmala, M., Worsnop, D.R., Thornton, J.A., Donahue, N., Kjaergaard, H.G. and Ehn, M. (2019) Highly oxygenated organic molecules (HOM) from gas-phase autoxidation involving peroxy radicals: A key contributor to atmospheric aerosol. Chemical Reviews 119(6), 3472-3509.
Boyd, A.A., Flaud, P.-M., Daugey, N. and Lesclaux, R. (2003) Rate Constants for RO2 + HO2 Reactions Measured under a Large Excess of HO2. The Journal of Physical Chemistry A 107(6), 818-821.
Corchnoy, S.B. and Atkinson, R. (1990) Kinetics of the Gas-Phase Reactions of OH and NO3 Radicals with 2-Carene,1,8-Cineole, p-Cymene, and Terpinolene. Environmental Science & Technology 24(10), 1497-1502.
Curtius, J., Heinritzi, M., Beck, L.J., Pöhlker, M.L., Tripathi, N., Krumm, B.E., Holzbeck, P., Nussbaumer, C.M., Hernández Pardo, L., Klimach, T., Barmpounis, K., Andersen, S.T., Bardakov, R., Bohn, B., Cecchini, M.A., Chaboureau, J.-P., Dauhut, T., Dienhart, D., Dörich, R., Edtbauer, A., Giez, A., Hartmann, A., Holanda, B.A., Joppe, P., Kaiser, K., Keber, T., Klebach, H., Krüger, O.O., Kürten, A., Mallaun, C., Marno, D., Martinez, M., Monteiro, C., Nelson, C., Ort, L., Raj, S.S., Richter, S., Ringsdorf, A., Rocha, F., Simon, M., Sreekumar, S., Tsokankunku, A., Unfer, G.R., Valenti, I.D., Wang, N., Zahn, A., Zauner-Wieczorek, M., Albrecht, R.I., Andreae, M.O., Artaxo, P., Crowley, J.N., Fischer, H., Harder, H., Herdies, D.L., Machado, L.A.T., Pöhlker, C., Pöschl, U., Possner, A., Pozzer, A., Schneider, J., Williams, J. and Lelieveld, J. (2024) Isoprene nitrates drive new particle formation in Amazon's upper troposphere. Nature 636(8041), 124-130.
Draper, D.C., Farmer, D.K., Desyaterik, Y. and Fry, J.L. (2015) A qualitative comparison of secondary organic aerosol yields and composition from ozonolysis of monoterpenes at varying concentrations of NO2. ATMOSPHERIC CHEMISTRY AND PHYSICS 15(21), 12267-12281.
Fouqueau, A., Cirtog, M., Cazaunau, M., Pangui, E., Doussin, J.F. and Picquet-Varrault, B. (2022) An experimental study of the reactivity of terpinolene and β-caryophyllene with the nitrate radical. ATMOSPHERIC CHEMISTRY AND PHYSICS 22(10), 6411-6434.
Friedman, B. and Farmer, D.K. (2018) SOA and gas phase organic acid yields from the sequential photooxidation of seven monoterpenes. Atmospheric Environment 187, 335-345.
Fry, J.L., Draper, D.C., Barsanti, K.C., Smith, J.N., Ortega, J., Winkler, P.M., Lawler, M.J., Brown, S.S., Edwards, P.M., Cohen, R.C. and Lee, L. (2014) Secondary Organic Aerosol Formation and Organic Nitrate Yield from NO3 Oxidation of Biogenic Hydrocarbons. Environmental Science & Technology 48(20), 11944-11953.
Garmash, O., Rissanen, M.P., Pullinen, I., Schmitt, S., Kausiala, O., Tillmann, R., Zhao, D., Percival, C., Bannan, T.J., Priestley, M., Hallquist, Å.M., Kleist, E., Kiendler-Scharr, A., Hallquist, M., Berndt, T., McFiggans, G., Wildt, J., Mentel, T.F. and Ehn, M. (2020) Multi-generation OH oxidation as a source for highly oxygenated organic molecules from aromatics. ATMOSPHERIC CHEMISTRY AND

PHYSICS 20(1), 515-537.
Griffin, R.J., Cocker, D.R., III, Flagan, R.C. and Seinfeld, J.H. (1999) Organic aerosol formation from the oxidation of biogenic hydrocarbons. Journal of Geophysical Research 104(D3), 3555-3567.
Guenther, A.B., Jiang, X., Heald, C.L., Sakulyanontvittaya, T., Duhl, T., Emmons, L.K. and Wang, X. (2012) The Model of Emissions of Gases and Aerosols from Nature version 2.1 (MEGAN2.1): an extended and updated framework for modeling biogenic emissions. Geosci. Model Dev. 5(6), 1471-1492.
Guo, Y., Yan, C., Liu, Y., Qiao, X., Zheng, F., Zhang, Y., Zhou, Y., Li, C., Fan, X., Lin, Z., Feng, Z., Zhang, Y., Zheng, P., Tian, L., Nie, W., Wang, Z., Huang, D., Daellenbach, K.R., Yao, L., Dada, L., Bianchi, F., Jiang, J., Liu, Y., Kerminen, V.M. and Kulmala, M. (2022) Seasonal variation in oxygenated organic molecules in urban Beijing and their contribution to secondary organic aerosol. ATMOSPHERIC CHEMISTRY AND PHYSICS 22(15), 10077-10097.
Hakola, H., Arey, J., Aschmann, S.M. and Atkinson, R. (1994) Product formation from the gas-phase reactions of OH radicals and O3 with a series of monoterpenes. Journal of Atmospheric Chemistry 18(1), 75-102.
Herrmann, F., Winterhalter, R., Moortgat, G.K. and Williams, J. (2010) Hydroxyl radical (OH) yields from the ozonolysis of both double bonds for five monoterpenes. Atmospheric Environment 44(28), 3458-3464.
Hofzumahaus, A., Rohrer, F., Lu, K., Bohn, B., Brauers, T., Chang, C.-C., Fuchs, H., Holland, F., Kita, K., Kondo, Y., Li, X., Lou, S., Shao, M., Zeng, L., Wahner, A. and Zhang, Y. (2009) Amplified Trace Gas Removal in the Troposphere. SCience 324(5935), 1702-1704.
Huang, X., Zhou, L., Ding, A., Qi, X., Nie, W., Wang, M., Chi, X., Petäjä, T., Kerminen, V.M., Roldin, P., Rusanen, A., Kulmala, M. and Boy, M. (2016) Comprehensive modelling study on observed new particle formation at the SORPES station in Nanjing, China. ATMOSPHERIC CHEMISTRY AND PHYSICS 16(4), 2477-2492.
Humphrey, W., Dalke, A. and Schulten, K. (1996) VMD: Visual molecular dynamics. Journal of Molecular Graphics 14(1), 33-38.
Isaacman-VanWertz, G. and Aumont, B. (2021) Impact of organic molecular structure on the estimation of atmospherically relevant physicochemical parameters. Atmos. Chem. Phys. 21(8), 6541-6563.
Kim, H. (2016) A Density Functional Theory Study on the Reaction Mechanism of Terpinolene with O3. Bulletin of the Korean Chemical Society 37(2), 121-122.
Kurtén, T., Møller, K.H., Nguyen, T.B., Schwantes, R.H., Misztal, P.K., Su, L., Wennberg, P.O., Fry, J.L. and Kjaergaard, H.G. (2017) Alkoxy Radical Bond Scissions Explain the Anomalously Low Secondary Organic Aerosol and Organonitrate Yields From α-Pinene + NO3. The Journal of Physical Chemistry Letters 8(13), 2826-2834.
Lee, A., Goldstein, A.H., Keywood, M.D., Gao, S., Varutbangkul, V., Bahreini, R., Ng, N.L., Flagan, R.C. and Seinfeld, J.H. (2006) Gas-phase products and secondary aerosol yields from the ozonolysis of ten different terpenes. Journal of Geophysical Research-Atmospheres 111(D7).
Lindwall, F., Faubert, P. and Rinnan, R. (2015) Diel Variation of Biogenic Volatile Organic Compound Emissions- A field Study in the Sub, Low and High Arctic on the Effect of Temperature and Light. PLOS ONE 10(4), e0123610.
Liu, Y., Liu, C., Nie, W., Li, Y., Ge, D., Chen, L., Zhu, C., Wang, L., Zhang, Y., Liu, T., Qi, X., Wang, J., Huang, D., Wang, Z., Yan, C., Chi, X. and Ding, A. (2023) Exploring condensable organic vapors and their co-occurrence with PM2.5 and O3 in winter in Eastern China. Environmental Science: Atmospheres 3(2), 282-297.

Liu, Y., Nie, W., Li, Y., Ge, D., Liu, C., Xu, Z., Chen, L., Wang, T., Wang, L., Sun, P., Qi, X., Wang, J., Xu, Z., Yuan, J., Yan, C., Zhang, Y., Huang, D., Wang, Z., Donahue, N.M., Worsnop, D., Chi, X., Ehn, M. and Ding, A. (2021) Formation of condensable organic vapors from anthropogenic and biogenic volatile organic compounds (VOCs) is strongly perturbed by NOx in eastern China. ATMOSPHERIC CHEMISTRY AND PHYSICS 21(19), 14789-14814.

Lu, T. and Chen, F. (2012) Multiwfn: A multifunctional wavefunction analyzer. 33(5), 580-592.

Luo, D.M., Pierce, J.A., Malkina, I.L. and Carter, W.P.L. (1996) Rate constants for the reactions of O(3P) with selected monoterpenes. International Journal of Chemical Kinetics 28(1), 1-8.

Luo, H., Vereecken, L., Shen, H., Kang, S., Pullinen, I., Hallquist, M., Fuchs, H., Wahner, A., Kiendler-Scharr, A., Mentel, T.F. and Zhao, D. (2023) Formation of highly oxygenated organic molecules from the oxidation of limonene by OH radical: significant contribution of H-abstraction pathway. ATMOSPHERIC CHEMISTRY AND PHYSICS 23(13), 7297-7319.

Ma, F., Guo, X., Xia, D., Xie, H.-B., Wang, Y., Elm, J., Chen, J. and Niu, J. (2021) Atmospheric Chemistry of Allylic Radicals from Isoprene: A Successive Cyclization-Driven Autoxidation Mechanism. Environmental Science & Technology 55(8), 4399-4409.

Martínez, E., Cabañas, B., Aranda, A., Martín, P. and Salgado, S. (1999) Absolute rate coefficients for the gas-phase reactions of NO3 radical with a series of monoterpenes at T=298 to 433 K. Journal of Atmospheric Chemistry 33(3), 265-282.

Mohr, C., Lopez-Hilfiker, F.D., Yli-Juuti, T., Heitto, A., Lutz, A., Hallquist, M., D'Ambro, E.L., Rissanen, M.P., Hao, L., Schobesberger, S., Kulmala, M., Mauldin III, R.L., Makkonen, U., Sipilä, M., Petäjä, T. and Thornton, J.A. (2017) Ambient observations of dimers from terpene oxidation in the gas phase: Implications for new particle formation and growth. Geophysical Research Letters 44(6), 2958-2966.

Mohr, C., Thornton, J.A., Heitto, A., Lopez-Hilfiker, F.D., Lutz, A., Riipinen, I., Hong, J., Donahue, N.M., Hallquist, M., Petäjä, T., Kulmala, M. and Yli-Juuti, T. (2019) Molecular identification of organic vapors driving atmospheric nanoparticle growth. Nature Communications 10(1), 4442.

Nie, W., Yan, C., Huang, D.D., Wang, Z., Liu, Y., Qiao, X., Guo, Y., Tian, L., Zheng, P., Xu, Z., Li, Y., Xu, Z., Qi, X., Sun, P., Wang, J., Zheng, F., Li, X., Yin, R., Dallenbach, K.R., Bianchi, F., Petäjä, T., Zhang, Y., Wang, M., Schervish, M., Wang, S., Qiao, L., Wang, Q., Zhou, M., Wang, H., Yu, C., Yao, D., Guo, H., Ye, P., Lee, S., Li, Y.J., Liu, Y., Chi, X., Kerminen, V.-M., Ehn, M., Donahue, N.M., Wang, T., Huang, C., Kulmala, M., Worsnop, D., Jiang, J. and Ding, A. (2022) Secondary organic aerosol formed by condensing anthropogenic vapours over China's megacities. Nature Geoscience 15(4), 255-261.

Nie, W., Yan, C., Yang, L., Roldin, P., Liu, Y., Vogel, A.L., Molteni, U., Stolzenburg, D., Finkenzeller, H., Amorim, A., Bianchi, F., Curtius, J., Dada, L., Draper, D.C., Duplissy, J., Hansel, A., He, X.-C., Hofbauer, V., Jokinen, T., Kim, C., Lehtipalo, K., Nichman, L., Mauldin, R.L., Makhmutov, V., Mentler, B., Mizelli-Ojdanic, A., Petäjä, T., Quéléver, L.L.J., Schallhart, S., Simon, M., Tauber, C., Tomé, A., Volkamer, R., Wagner, A.C., Wagner, R., Wang, M., Ye, P., Li, H., Huang, W., Qi, X., Lou, S., Liu, T., Chi, X., Dommen, J., Baltensperger, U., El Haddad, I., Kirkby, J., Worsnop, D., Kulmala, M., Donahue, N.M., Ehn, M. and Ding, A. (2023) NO at low concentration can enhance the formation of highly oxygenated biogenic molecules in the atmosphere. Nature Communications 14(1), 3347.

Orlando, J.J., Nozière, B., Tyndall, G.S., Orzechowska, G.E., Paulson, S.E. and Rudich, Y. (2000) Product studies of the OH- and ozone-initiated oxidation of some monoterpenes. Journal of Geophysical Research-Atmospheres 105(D9), 11561-11572.

Orzechowska, G.E. (2003) Atmospheric chemistry of ozone reactions with alkenes.

Pankow, J.F. and Asher, W.E. (2008) SIMPOL.1: a simple group contribution method for predicting

vapor pressures and enthalpies of vaporization of multifunctional organic compounds. ATMOSPHERIC CHEMISTRY AND PHYSICS 8(10), 2773-2796.
Peeters, J., Müller, J.-F., Stavrakou, T. and Nguyen, V.S. (2014) Hydroxyl Radical Recycling in Isoprene Oxidation Driven by Hydrogen Bonding and Hydrogen Tunneling: The Upgraded LIM1 Mechanism. The Journal of Physical Chemistry A 118(38), 8625-8643.
Qiao, X.H., Li, X.X., Yan, C., Sarnela, N., Yin, R.J., Guo, Y.S., Yao, L., Nie, W., Huang, D.D., Wang, Z., Bianchi, F., Liu, Y.C., Donahue, N.M., Kulmala, M. and Jiang, J.K. (2023) Precursor apportionment of atmospheric oxygenated organic molecules using a machine learning method. ENVIRONMENTAL SCIENCE-ATMOSPHERES 3(1), 230-237.
Reissell, A., Harry, C., Aschmann, S.M., Atkinson, R. and Arey, J. (1999) Formation of acetone from the OH radical- and O3-initiated reactions of a series of monoterpenes. Journal of Geophysical Research-Atmospheres 104(D11), 13869-13879.
Rollins, A.W., Pusede, S., Wooldridge, P., Min, K.E., Gentner, D.R., Goldstein, A.H., Liu, S., Day, D.A., Russell, L.M., Rubitschun, C.L., Surratt, J.D. and Cohen, R.C. (2013) Gas/particle partitioning of total alkyl nitrates observed with TD-LIF in Bakersfield. Journal of Geophysical Research: Atmospheres 118(12), 6651-6662.
Saunders, S.M., Jenkin, M.E., Derwent, R.G. and Pilling, M.J. (2003) Protocol for the development of the Master Chemical Mechanism, MCM v3 (Part A): tropospheric degradation of non-aromatic volatile organic compounds. ATMOSPHERIC CHEMISTRY AND PHYSICS 3(1), 161-180.
Shen, H., Vereecken, L., Kang, S., Pullinen, I., Fuchs, H., Zhao, D. and Mentel, T.F. (2022) Unexpected significance of a minor reaction pathway in daytime formation of biogenic highly oxygenated organic compounds. Science Advances 8(42), eabp8702.
Shu, Y. and Atkinson, R. (1994) Rate constants for the gas-phase reactions of O3 with a series of Terpenes and OH radical formation from the O3 reactions with Sesquiterpenes at 296 ± 2 K. International Journal of Chemical Kinetics 26(12), 1193-1205.
Stewart, D.J., Almabrok, S.H., Lockhart, J.P., Mohamed, O.M., Nutt, D.R., Pfrang, C. and Marston, G. (2013) The kinetics of the gas-phase reactions of selected monoterpenes and cyclo-alkenes with ozone and the NO3 radical. Atmospheric Environment 70, 227-235.
Surratt, J.D., Gómez-González, Y., Chan, A.W.H., Vermeylen, R., Shahgholi, M., Kleindienst, T.E., Edney, E.O., Offenberg, J.H., Lewandowski, M., Jaoui, M., Maenhaut, W., Claeys, M., Flagan, R.C. and Seinfeld, J.H. (2008) Organosulfate formation in biogenic secondary organic aerosol. The Journal of Physical Chemistry A 112(36), 8345-8378.
Tröstl, J., Chuang, W.K., Gordon, H., Heinritzi, M., Yan, C., Molteni, U., Ahlm, L., Frege, C., Bianchi, F., Wagner, R., Simon, M., Lehtipalo, K., Williamson, C., Craven, J.S., Duplissy, J., Adamov, A., Almeida, J., Bernhammer, A.-K., Breitenlechner, M., Brilke, S., Dias, A., Ehrhart, S., Flagan, R.C., Franchin, A., Fuchs, C., Guida, R., Gysel, M., Hansel, A., Hoyle, C.R., Jokinen, T., Junninen, H., Kangasluoma, J., Keskinen, H., Kim, J., Krapf, M., Kürten, A., Laaksonen, A., Lawler, M., Leiminger, M., Mathot, S., Möhler, O., Nieminen, T., Onnela, A., Petäjä, T., Piel, F.M., Miettinen, P., Rissanen, M.P., Rondo, L., Sarnela, N., Schobesberger, S., Sengupta, K., Sipilä, M., Smith, J.N., Steiner, G., Tomè, A., Virtanen, A., Wagner, A.C., Weingartner, E., Wimmer, D., Winkler, P.M., Ye, P., Carslaw, K.S., Curtius, J., Dommen, J., Kirkby, J., Kulmala, M., Riipinen, I., Worsnop, D.R., Donahue, N.M. and Baltensperger, U. (2016) The role of low-volatility organic compounds in initial particle growth in the atmosphere. Nature 533(7604), 527-531.
Valorso, R., Aumont, B., Camredon, M., Raventos-Duran, T., Mouchel-Vallon, C., Ng, N.L., Seinfeld,

J.H., Lee-Taylor, J. and Madronich, S. (2011) Explicit modelling of SOA formation from α-pinene photooxidation: sensitivity to vapour pressure estimation. ATMOSPHERIC CHEMISTRY AND PHYSICS 11(14), 6895-6910.
Vasudevan-Geetha, V., Tiszenkel, L., Wang, Z., Russo, R., Bryant, D., Lee-Taylor, J., Barsanti, K. and Lee, S.H. (2024) Isomer Molecular Structures and Formation Pathways of Oxygenated Organic Molecules in Newly Formed Biogenic Particles. EGUsphere 2024, 1-20.
Wang, J., Feng, L., Palmer, P.I., Liu, Y., Fang, S., Bösch, H., O'Dell, C.W., Tang, X., Yang, D., Liu, L. and Xia, C. (2020) Large Chinese land carbon sink estimated from atmospheric carbon dioxide data. Nature 586(7831), 720-723.
Wang, S. and Wang, L. (2016) The atmospheric oxidation of dimethyl, diethyl, and diisopropyl ethers. The role of the intramolecular hydrogen shift in peroxy radicals. Physical Chemistry Chemical Physics 18(11), 7707-7714.
Wang, Y., Clusius, P., Yan, C., Dällenbach, K., Yin, R., Wang, M., He, X.-C., Chu, B., Lu, Y., Dada, L., Kangasluoma, J., Rantala, P., Deng, C., Lin, Z., Wang, W., Yao, L., Fan, X., Du, W., Cai, J., Heikkinen, L., Tham, Y.J., Zha, Q., Ling, Z., Junninen, H., Petäjä, T., Ge, M., Wang, Y., He, H., Worsnop, D.R., Kerminen, V.-M., Bianchi, F., Wang, L., Jiang, J., Liu, Y., Boy, M., Ehn, M., Donahue, N.M. and Kulmala, M. (2022) Molecular Composition of Oxygenated Organic Molecules and Their Contributions to Organic Aerosol in Beijing. Environmental Science & Technology 56(2), 770-778.
Witter, M., Berndt, T., Böge, O., Stratmann, F. and Heintzenberg, J. (2002) Gas-phase ozonolysis:: Rate coefficients for a series of terpenes and rate coefficients and OH yields for 2-methyl-2-butene and 2,3-dimethyl-2-butene. International Journal of Chemical Kinetics 34(6), 394-403.
Wu, R., Wang, S. and Wang, L. (2015) New Mechanism for the Atmospheric Oxidation of Dimethyl Sulfide. The Importance of Intramolecular Hydrogen Shift in a CH3SCH2OO Radical. The Journal of Physical Chemistry A 119(1), 112-117.
Zheng, P., Chen, Y., Wang, Z., Liu, Y., Pu, W., Yu, C., Xia, M., Xu, Y., Guo, J., Guo, Y., Tian, L., Qiao, X., Huang, D.D., Yan, C., Nie, W., Worsnop, D.R., Lee, S. and Wang, T. (2023) Molecular Characterization of Oxygenated Organic Molecules and Their Dominating Roles in Particle Growth in Hong Kong. Environmental Science & Technology 57(20), 7764-7776.

Graphical Abstract

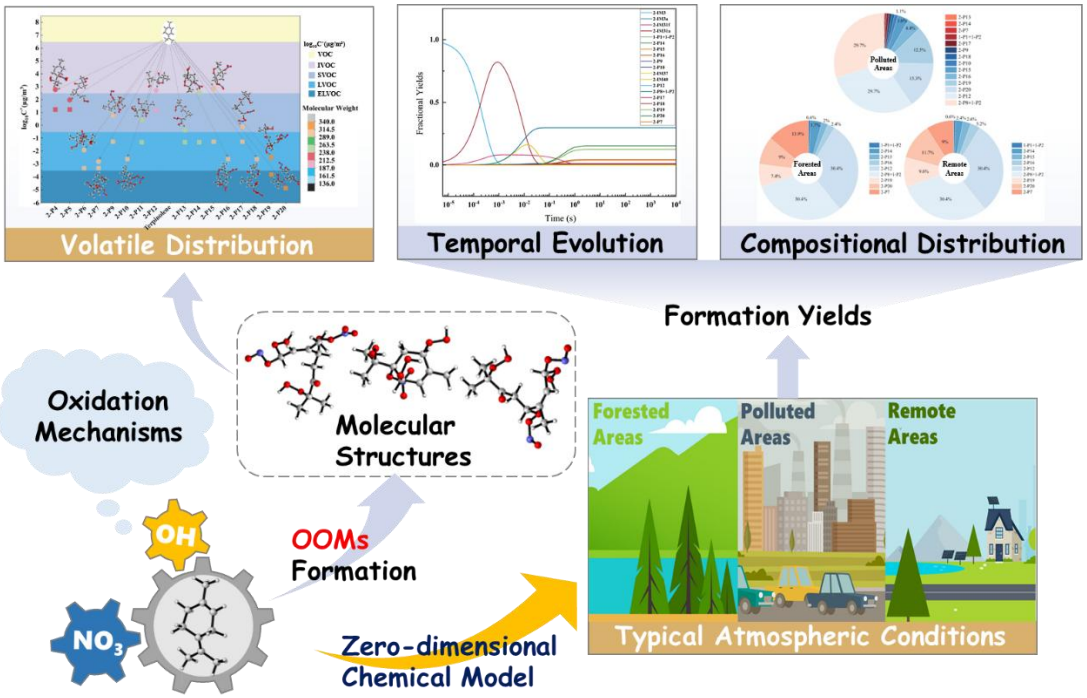
Volatile Distribution
Temporal Evolution
Compositional Distribution
Formation Yields
Oxidation Mechanisms
Molecular Structures
OOMs Formation
Zero-dimensional Chemical Model
Forested Areas
Polluted Areas
Remote Areas
Typical Atmospheric Conditions

699